Particle
& Particle Systems Characterization
www.particle-journal.com



# Gold Spiky Nanodumbbells: Anisotropy in Gold Nanostars

*Sergey M. Novikov, Ana Sánchez-Iglesias, Mikołaj K. Schmidt, Andrey Chuvilin, Javier Aizpurua, Marek Grzelczak, and Luis M. Liz-Marzán**

Interaction of light with nanostructured materials and nanostructures gives rise to a variety of fascinating optical phenomena at the nanoscale. One of the most remarkable effects in light scattering by metal nanostructures is the strong electromagnetic field enhancement (FE) up to several orders of magnitude and spatially localized on the nanometer scale. Such an enhancement occurs due to the resonantly excited collective electron oscillations, known as localized surface plasmons (LSPs).[1,2] LSPs are highly sensitive to the geometry, material, and surrounding medium of metal nanostructures.[2] The FE is extremely important for practical applications such as sensors,[3–5] or micro-optical devices,[6] and plays a major role in surface-enhanced Raman scattering (SERS).[7–9]

Among many shapes available for gold nanoparticles, rod- and star-like morphologies are expected to find wide applications in a variety of plasmon-oriented technologies. The shape anisotropy of nanorods leads to strong differences in optical absorption as a function of the polarization of incident light, which has been applied for example in high-density optical recording.[10] Nanostars, on the other hand, can spatially focus the incoming light by means of electric FE around their spikes. Such an enhancement allows the use of the stars for detection, even at the single-molecule level.[11–13] Thus, it is rather obvious that combination of both shapes within one nanostructure can provide unconventional optical response, with even wider applicability. Although self-assembly of these two shapes into new systems could be a convenient pathway to produce complex plasmonic structures, the difficulty in surface functionalization by suitable (macro)molecules makes this strategy rather challenging. Thus, recent advancements in tip-overgrowth of gold nanorods (AuNRs)[14,15] provide an attractive synthetic toolbox to develop novel plasmonic nanoparticles that combine the characteristic optical properties of both AuNRs and gold nanostars.

Here we introduce a new type of gold nanoparticle that we call "spiky nanodumbbells" (AuSNDs), which comprise a AuNR with multiple spikes protruding from each end (**Figure 1**). The synthesis of such nanoparticles is based on the seeded growth method, by chemical reduction of a gold salt on preformed AuNRs.[16] The reduction was carried out following the same method as previously reported for the growth of gold nanostars, by introducing the AuNRs in a solution of poly(*N*-vinylpyrrolidone) (PVP) in *N*,*N*-dimethylformamide (DMF) and then adding $HAuCl_4$.[17] As a result, growth at the ends of the AuNRs takes place in the form of multiple spikes. The extent of spike growth can be controlled through the amount of gold reduced on the AuNRs, from only few small spikes up to a morphology resembling two closely spaced nanostars (Figure 1b,c). Interestingly, the growth of spikes on the AuNRs is accompanied by significant changes in the optical response. The spectrum of AuNRs is known to display a longitudinal mode (around 850 nm in this case), and a transverse mode (around 520 nm). The growth of spikes at the AuNR ends leads to a significant redshift of the longitudinal resonance mode, while the transverse mode gets broader, more intense and also slightly redshifted, and a new resonance arises around 780 nm (Figure 1). When the spikes have grown larger and the central rod can no longer be recognized, we can only distinguish (in the spectral range accessible for measurements) a broad resonance around 850 nm and a shoulder near 590 nm (Figure 1), which are typical for Au nanostars.[13]

Since UV–vis–NIR spectra from solution provide an average over all the particles and orientations, the optical properties of individual particles were studied by dark-field optical microspectroscopy (DFM).[18,19] For DFM measurements, AuSNDs were deposited by spin coating on an indium tin oxide (ITO; 10 nm thick)-coated glass slide. The optimum concentration of particles and spinning rate were matched to provide a minimum distance between nanoparticles of 3–5 μm, to ensure that the optical signature of single particles can be recorded. The slides contain well-defined marks, which allow us to unequivocally determine the position of the each particle and correlate scanning electron microscopy (SEM) and DFM data.[20] **Figure 2** shows scattering dark-field spectra from an individual AuSND, as well as an SEM image of the same particle. The SEM image shows a coating layer around the particle, which results from the deposition of organic material under the SEM electron beam. It should be noted that this coating does not affect the optical properties of the particle, since SEM imaging was carried out after recording the scattering spectra. The dark-field spectrum for this particle shows two pronounced resonances at 582 and 774 nm, which was found to be a general feature for the scattering dark-field spectra measured for at least 10 particles (additional examples are shown in the Supporting Information, Figure S1). The positions of these resonances are in good agreement with the corresponding ensemble UV–vis spectrum, but the spectral range limitations for our setup (400–950 nm) do not allow us to analyze the NIR region

Dr. S. M. Novikov, A. Sánchez-Iglesias,
Dr. M. Grzelczak, Prof. L. M. Liz-Marzán
Bionanoplasmonics Laboratory
CIC biomaGUNE, Paseo de Miramón 182
20009 Donostia-San Sebastián, Spain
E-mail: llizmarzan@cicbiomagune.es
M. K. Schmidt, Dr. J. Aizpurua
Centro de Física de Materiales CSIC-UPV/EHU
and Donostia International Physics Center DIPC
Paseo Manuel de Lardizabal 5, 20018 Donostia-San Sebastián, Spain
Dr. A. Chuvilin
CIC nanoGUNE Consolider
Av. de Tolosa 76, 20018 Donostia-San Sebastián, Spain
Dr. A. Chuvilin, Dr. M. Grzelczak, Prof. L. M. Liz-Marzán
Ikerbasque, Basque Foundation for Science, 48011 Bilbao, Spain

**DOI: 10.1002/ppsc.201300257**

Particle
& Particle Systems Characterization
www.particle-journal.com

Materials Views
www.MaterialsViews.com

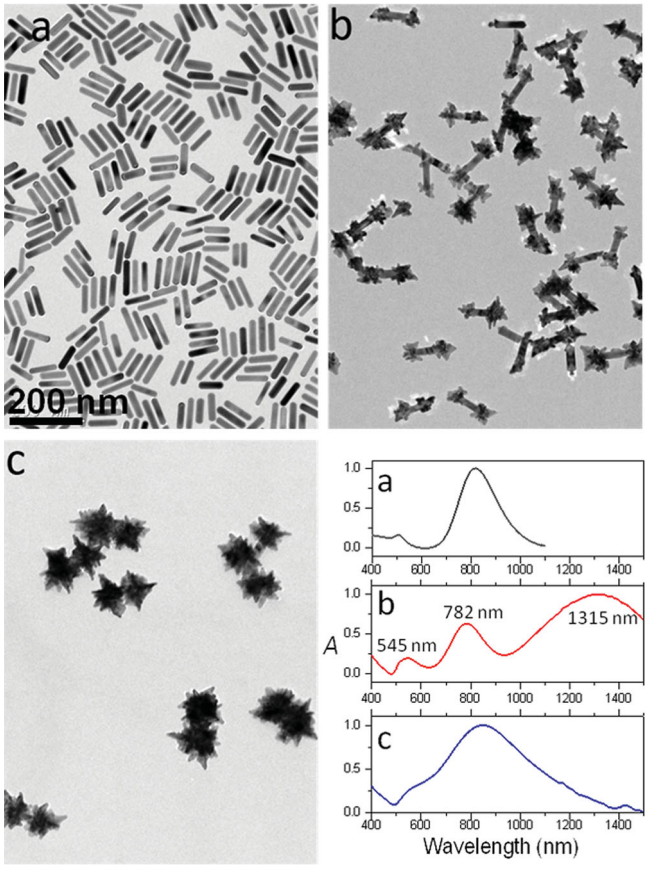


**Figure 1.** TEM images of synthesized gold nanoparticles: a) nanorods, b) spiky nanodumbbells (SNDs), c) SNDs resembling two closely spaced nanostars. The corresponding UV–vis–NIR spectra of the colloidal dispersions of these particles are also shown. The labels indicate the particles from which each spectrum was measured.

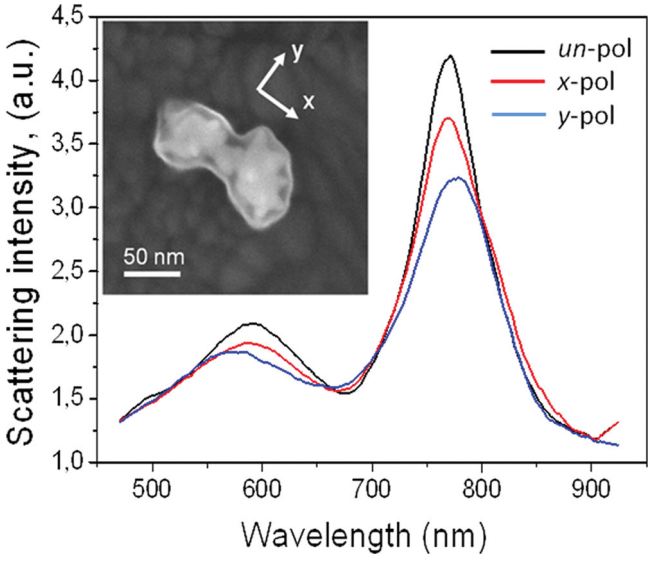


**Figure 2.** Experimental dark-field scattering spectra of an individual spiky nanodumbbell. Polarization of the incident light is indicated by the labels. Inset: SEM image of the particle from which the DFM spectra were recorded.

and accordingly the resonance near 1200 nm. The minor differences between resonance positions in the ensemble UV–vis and DFM spectra reflect the deviations of the specific morphology of each nanoparticle with respect to the average, but also the different dielectric environment, which in the DFM configuration is defined by air and the glass/ITO substrate. DFM also allowed us to study the polarization dependence of the optical response of single particles, by performing measurements in which the incident light was polarized along the *x*- (red curve) and *y*- (blue curve) axes of the particle (as marked in the inset). Non-polarized detection was used to ensure a sufficient signal-to-noise ratio. For both polarization directions, the resonances almost coincide with those recorded under non-polarized illumination. However, in the case of *y*-polarization, the intensities of both peaks are slightly lower than those for *x*-polarization, with a more pronounced damping for the peak near 582, which is also slightly blueshifted.

To understand the nature of the experimentally determined resonances, the finite-difference time-domain (FDTD) method was used to calculate light scattering and extinction spectra by AuSNDs (**Figure 3**). To ensure the accuracy of our results, we used an inhomogeneous mesh with 0.5 nm minimum lateral size in the proximity of the nanostructure, and verified that this refinement, as well as the allowed evolution in time, provided convergent results. The numerical modeling was made for a system on the basis of a cylinder terminated by two spheres at the ends, which were then decorated with randomly oriented blunted conical spikes (Figure 3a, inset). The dimensions of the particle used for these calculations were established from electron microscopy data (see Table S1, Supporting Information). The calculations were performed for two polarization directions, along (black curve) and perpendicular (red curve) to the particle with normal illumination in a homogeneous environment (medium refractive index = 1.43), and the dielectric function of gold was taken from the literature.[21] The calculated spectra show two peaks at 1200 and 800 nm, as well as

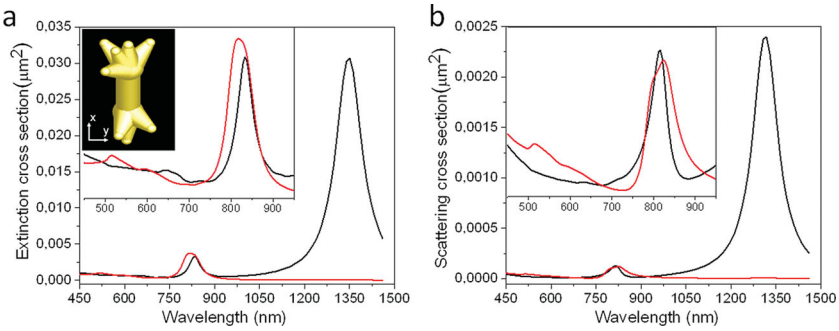


**Figure 3.** Calculated spectra of a single AuSND (inset in a) for *x*-polarization (black curve) and *y*-polarization (red curve). The directions are indicated in the inset. a) Extinction cross-section spectra. b) Scattering cross-section spectra. The insets show enlarged spectra in the region from 450 to 950 nm.




DOI: 10.1002/ppsc.201300257

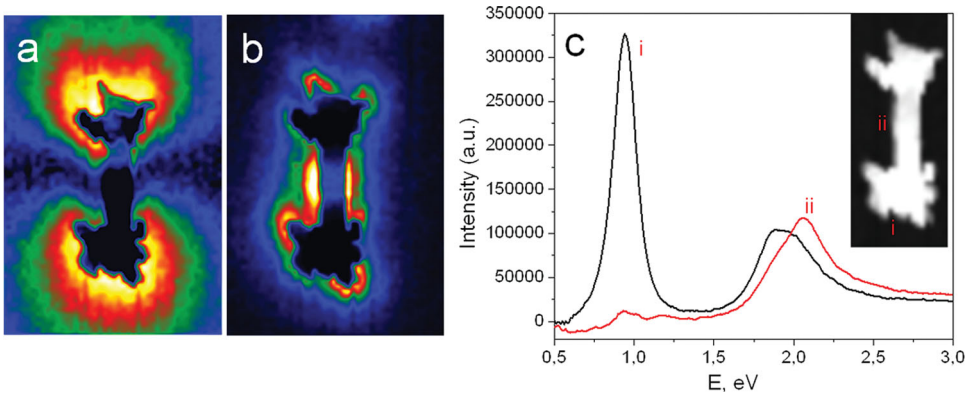


**Figure 4.** Plasmon maps obtained experimentally from the integrated EELS signal intensity over the energy range: a) 0.95–1.05 eV, b) 2–2.1 eV. c) EEL spectra were determined from the end (i-black curve) and near the middle (ii-red curve) of the AuSND, as indicated on the STEM image in the inset.

a shoulder at 520–580 nm. The pronounced peak at 1200 nm is identified as the longitudinal dipolar mode of the elongated nanostructures,[22,23] since for transverse polarization this peak is not present. Additionally, the same LSP resonance was calculated for an AuNR with the same overall dimensions (data not shown). The intermediate resonance at 800 nm can be observed for both polarization directions, meaning that it corresponds to the plasmon mode localized at the end caps of the nanostructure, which was confirmed by simulations of single-isolated spheres randomly decorated with spikes (Figure S2, Supporting Information). The broad resonance at 520–580 nm is the result of several contributions and can also be observed for both polarizations. The transverse resonance is localized in the central part of the nanorod and has a peak at 520 nm, while the spheres forming the endings of the central nanorod have an LSP at 510 nm. In addition, the spikes have quadrupolar resonances near 670 nm, which are present for both polarizations. The minor deviation between resonance positions in theory and experiment can be explained by the differences in morphological details between the ideal nanoparticle model (Figure 3 inset) and the real AuSNDs, since the positions of all resonances depend on the size of particle, but also on details such as the density and orientation of the spikes. Despite of these simplifications of the model, the calculated spectra qualitatively match the experimental data and clarify the origin of the observed LSP resonances.

We finally used electron energy loss spectral imaging (EELSI)[24,25] to experimentally determine the spatial distribution of LSP resonances in AuSNDs, and a representative example is shown in **Figure 4**. The loss intensity maps obtained from integrated EELS signal (Figure 4a,b) and extracted EEL spectra (Figure 4c) clearly show the distribution of plasmon resonances and the position of the peaks, respectively. Figure 4 presents intensity distributions and EEL spectra measured at the end (i) and near the edge of the central rod (ii) of an AuSND, as indicated in the STEM image (Figure 4c, inset). The positions [(i) and (ii)] of the LSP resonances in the EEL spectra are in good agreement with results obtained by both optical characterization and theoretical calculations. Spectra of local FE at positions (i) and (ii), shown in the Supporting Information (Figure S3), confirm the nature of the modes displayed in Figure 4 and indicate the potential of SNDs to generate large-field enhancements.

In conclusion, we have devised, fabricated, and characterized a new type of colloidal gold nanoparticles—spiky nanodumbbells. This type of particles combines shape anisotropy with sharp nanoscale features, which is reflected in their intricate optical response. The optical properties of the particles were studied by means of UV–vis–NIR spectroscopy, dark-field optical microspectroscopy, and electron energy loss spectroscopy, which provide an overall complete picture. Additionally, the FDTD method was used to theoretically describe the obtained experimental spectra, providing a first indication of the various LSP modes present in these nanoparticles. We believe that these new nanostructures will be of interest to the wide nanoplasmonics community and useful for sensing and biological applications, among others.

## Experimental Section

*Chemicals*: $HAuCl_4 \cdot 3H_2O$, cetyltrimethylammonium bromide (CTAB), sodium borohydride ($NaBH_4$), ascorbic acid, silver nitrate ($AgNO_3$), polyvinylpyrrolidone (PVP; average MW = 10 000), and *N,N*-dimethylformamide (DMF) were purchased from Sigma–Aldrich. All reactants were used without further purification.

*Synthesis of Gold Nanorods*:[16] Gold seeds were prepared by $NaBH_4$ ($10 \times 10^{-3}$ M, 0.3 mL) reduction of $HAuCl_4$ ($0.25 \times 10^{-3}$ M, 5 mL) in aqueous CTAB solution ($100 \times 10^{-3}$M). An aliquot of seeds solution (24 µL) was added to a growth solution (10 mL) containing CTAB ($100 \times 10^{-3}$ M), $HAuCl_4$ ($0.5 \times 10^{-3}$ M), ascorbic acid ($0.8 \times 10^{-3}$M), $AgNO_3$ ($0.12 \times 10^{-3}$ M), and HCl ($19 \times 10^{-3}$ M). The mixture was left undisturbed for 2 h at 30 °C. The solution (10 mL) was then centrifuged twice (8000 rpm, 30 min) to remove excess silver salt, ascorbic acid, and HCl, and redispersed in Milli-Q water; the final concentration of AuNRs in the colloid used for further growth was $3.5 \times 10^{-3}$ M. The average thickness was 15 nm and the average length 67 nm, as determined by TEM.

*Synthesis of Gold Spiky Nanodumbbells (AuSNDs)*:[17] For the growth of AuSNDs, 13.7 µL of an aqueous solution of 0.10 M $HAuCl_4$ was mixed with 5 mL of $10 \times 10^{-3}$ M PVP solution in DMF, the mixture was stirred until complete disappearance of the $Au^{+3}$ CTTS band at 325 nm, followed by rapid addition of preformed AuNRs in water (19.8 and 78.6 µL for the two samples, $[Au] = 3.5 \times 10^{-3}$ M) under stirring. Within 2 h at room temperature, a color change from colorless to blue indicates the formation of AuSNDs.

TEM images were obtained with a JEOL 2100-F transmission electron microscope operating at an acceleration voltage of 200 kV. Samples for TEM were centrifuged at 5000 rpm and redispersed in ethanol several times to decrease PVP concentration. Optical characterization of AuSNDs in solution was carried out by UV–vis–NIR spectroscopy

on a Cary 5000 spectrophotometer. Optical properties of individual AuSNDs were determined using DFM. The experimental setup is based on a commercial Nikon Eclipse Ti-U inversion microscope, coupled to a Spectra Pro 2150i and Pixis 1024 Acton thermoelectrically cooled charge-coupled device (CCD) (Princeton Instruments). We used a dark-field condenser (NA = 0.8 – 0.95), and ×100 objective (oil immersion, NA = 0.50). EELS maps were acquired on a Titan 60–300 (TM) electron microscope (FEI, Netherlands) equipped with high-brightness electron emitter (xFEG), monochromator, and Quantum (TM) electron energy loss spectrometer (Gatan, USA). Spectral images were acquired in monochromated STEM mode at 80 kV and processed in Digital Micrograph software using homemade scripts. Samples for EELS mapping were prepared by drop-casting a solution onto 15-nm thick PELCO Silicon Nitride Support Film (Ted Pella, USA) and drying on air. The numerical modeling of optical spectra was made using the FDTD method. This method provides information on the far-field properties of the nanoparticles—such as the scattering and absorption cross sections—as well as the near-field distribution around the nanostructure, including the local enhancement of the fields. In FDTD, the response of the nanoparticle to the plane wave illumination is obtained by time-tracing the evolution of the electromagnetic field in the system.

## Supporting Information

Supporting Information is available from the Wiley Online Library or from the author.

## Acknowledgements

This work has been funded by the European Research Council (ERC Advanced Grant #267867 Plasmaquo). M.K.S. and J.A. acknowledge funding from the ETORTEK project nanoIKER of the Department of Industry of the Government of the Basque Country and project FIS2010–19609-C02–01 of the Spanish Ministry of Innovation.

Received: July 26, 2013
Revised: August 14, 2013
Published online:

[1] M. Pelton, J. Aizpurua, G. W. Bryant, *Laser Photon. Rev.* **2008**, *2*, 136.
[2] N. J. Halas, S. Lal, W.-S. Chang, S. Link, P. Nordlander, *Chem. Rev.* **2011**, *111*, 3913.
[3] A. D. McFarland, R. P. Van Duyne, *Nano Lett.* **2003**, *3*, 1057.
[4] N. Liu, T. Weiss, M. Mesch, L. Langguth, U. Eigenthaler, M. Hirscher, C. Sönnichsen, H. Giessen, *Nano Lett.* **2010**, *10*, 1103.
[5] E. Ringe, B. Sharma, A.-I. Henry, L. D. Marks, R. P. V. Duyne, *Phys. Chem. Chem. Phys.* **2013**, *15*, 4110.
[6] I. P. Radko, V. S. Volkov, J. Beermann, A. B. Evlyukhin, T. Søndergaard, A. Boltasseva, S. I. Bozhevolnyi, *Laser Photon. Rev.* **2009**, *3*, 575.
[7] J. Beermann, S. M. Novikov, O. Albrektsen, M. G. Nielsen, S. I. Bozhevolnyi, *J. Opt. Soc. Am. B* **2009**, *26*, 2370.
[8] R. A. Alvarez-Puebla, L. M. Liz-Marzán, *Small* **2010**, *6*, 604.
[9] D. Cialla, A. März, R. Böhme, F. Theil, K. Weber, M. Schmitt, J. Popp, *Anal. Bioanal. Chem.* **2012**, *403*, 27.
[10] P. Zijlstra, J. W. M. Chon, M. Gu, *Nature* **2009**, *459*, 410.
[11] S. Nie, S. R. Emory, *Science* **1997**, *275*, 1102.
[12] K. Kneipp, Y. Wang, H. Kneipp, L. T. Perelman, I. Itzkan, R. R. Dasari, M. S. Feld, *Phys. Rev. Lett.* **1997**, *78*, 1667.
[13] A. Guerrero-Martínez, S. Barbosa, I. Pastoriza-Santos, L. M. Liz-Marzán, *Curr. Opin. Colloid Interface Sci.* **2011**, *16*, 118.
[14] Y. Xiang, X. Wu, D. Liu, L. Feng, K. Zhang, W. Chu, W. Zhou, S. Xie, *J. Phys. Chem. C* **2008**, *112*, 3203.
[15] M. Grzelczak, A. Sánchez-Iglesias, B. Rodríguez-González, R. Alvarez-Puebla, J. Pérez-Juste, L. M. Liz-Marzán, *Adv. Funct. Mater.* **2008**, *18*, 3780.
[16] M. Liu, P. Guyot-Sionnest, *J. Phys. Chem. B* **2005**, *109*, 22192.
[17] P. S. Kumar, I. Pastoriza-Santos, B. Rodríguez-González, F. J. García de Abajo, L. M. Liz-Marzán, *Nanotechnology* **2008**, *19*, 015606.
[18] L. Gunnarsson, T. Rindzevicius, J. Prikulis, B. Kasemo, M. Käll, S. Zou, G. C. Schatz, *J. Phys. Chem. B* **2005**, *109*, 1079.
[19] O. L. Muskens, V. Giannini, J. A. Sánchez-Gil, J. Gómez Rivas, *Opt. Express* **2007**, *15*, 17736.
[20] C. Novo, A. Funston, I. Pastoriza-Santos, L. M. Liz-Marzán, P. Mulvaney, *Angew. Chem Int. Ed.* **2007**, *46*, 3517.
[21] P. Johnson, R. W. Christy, *Phys. Rev. B* **1972**, *6*, 4370.
[22] S. Link, M. A. El-Sayed, *J. Phys. Chem. B* **1999**, *103*, 8410.
[23] G. W. Bryant, F. J. Garcia de Abajo, J. Aizpurua, *Nano Lett.* **2008**, *8*, 631.
[24] A. L. Koh, A. I. Fernández-Domínguez, D. W. McComb, S. A. Maier, J. K. W. Yang, *Nano Lett.* **2011**, *11*, 1323.
[25] S. Mazzucco, O. Stéphan, C. Colliex, I. Pastoriza-Santos, L. M. Liz-Marzán, J. Garcia de Abajo, M. Kociak, *Eur. Phys. J. Appl. Phys.* **2011**, *54*, 33512.